Evolution of Fracture Permeability Through Reactive Flow at Elevated Temperatures

Hideaki Yasuhara[1*], Amir Polak[2], Yasuhiro Mitani[3], Avrami Grader[1], Phillip Halleck[1] and Derek Elsworth[1]

*Corresponding Author: huy103@psu.edu
[1]Energy Institute and Department of Energy and Geo-Environmental Engineering,
Pennsylvania State University, PA, USA
[2]Departement of Civil and Environmental Engineering, Technion,
Israel Institute of Technology, Haifa, Israel
[3]Institute of Environmental Systems, Kyushu University, Hukuoka, Japan

Keywords
Fracture permeability, dissolution, precipitation, geochemistry

ABSTRACT

Flow-through experiments are conducted on a natural fracture in novaculite at a constant effective stress of 1.38 MPa and at staged temperatures of 20, 40, 80, and 120 °C. Fluid and mineral effluxes are measured throughout the 3150-hr experiment, together with post-experiment imaging by X-ray CT and destructive fracture-casting by Wood's metal impregnation. These measurements are used to constrain the evolution of dissolution-driven changes in fracture structure, and related permeability under hydrothermal conditions. At 20 °C the fracture aperture monotonically decreases from an initial aperture of 18.5 μm to 7.5 μm during the first 1494 hrs. This reduction is attributed to removal of mineral mass from bridging asperities. Subsequently, fracture aperture increases to 13 μm and is interpreted as a switching of dominant dissolution processes to free-face etching of the fracture void surfaces. The resulting rate of gaping increases with an increase in temperature. Post-experiment imaging by X-ray CT and by using the fracture cast independently constrains the resulting architecture of the evolved fracture porosity. No localized flow channel is apparent, despite the evolving hydraulic response which is suggestive of an evolving dissolution channel.

Introduction

An understanding of how the flow and transport characteristics of rock fractures evolve in time is crucial for the effective development of hydrothermal, and especially EGS, reservoirs. The influence of mechanical and chemical effects on the permeability of fractured reservoirs is well recognized, however the interaction between mechanical and chemical influences remains ill-constrained. To date, no conclusive view exists of the evolution in fracture permeability when arbitrary stresses, temperatures, and chemical potentials are applied – specifically whether permeability will increase or reduce under net dissolution. Reduction is driven as bridging asperities are removed and/or secondary minerals are reprecipitated (i.e., pressure dissolution). Permeability increase is driven as the fracture void is etched by net dissolution (i.e., free-face dissolution). Sealing, likely driven by pressure solution, results from either removal of bridging asperities or mineral precipitation, is reported in some instances at elevated temperature (>300°C) [Moore *et al.*, 1994; Kanagawa, *et al.*, 2000; Morrow *et al.*, 2001; Tenthorey *et al.*, 2003; Hilgers and Tenthorey, 2004], at modest temperature (50 – 150°C) [Lin *et al.*, 1997; Polak *et al*, 2003; Dobson *et al.*, 2004], and under low effective stress (0.2 MPa) with an acidic solution [Durham *et al.*, 2001]. Conversely, gaping driven by free-face dissolution is suggested in carbonate reservoirs [e.g., Liu *et al.*, *1997*], and in the development of karst [e.g., Palmer, *1991*]. Importantly, these opposing behaviors may operate concurrently, but to varying degrees. Subtle changes in local conditions of applied stress, temperature or chemical potential may trigger switching between dominant mechanisms. Thus, besides monotonic sealing or gaping of a fracture, the behavior may switch, either in response to changing stress, temperature or chemical conditions, or spontaneously, with no apparent trigger [Polak, *et al.*, 2004].

This study examines changes in permeability with net dissolution that proceeds within a natural fracture in Arkansas novaculite. Specifically, our focus is placed on defining the critical factors controlling the overall behavior; fracture gaping or closing. Experimental measurements of evolving fluid pressure differential between sample inlet and outlet, prescribed flow rates and confining pressure, and non-destructive CT images of the fracture, are used to constrain the evolution of fracture porosity. Final fracture void morphology is anchored by a Wood's metal cast of the fracture. These ensemble observations are used to constrain the competing processes that contribute to permeability augmentation and reduction.

Experimental Method

The flow-through experiment (Figure 1) was conducted on a cylindrical sample of Arkansas novaculite (50.0 mm diameter

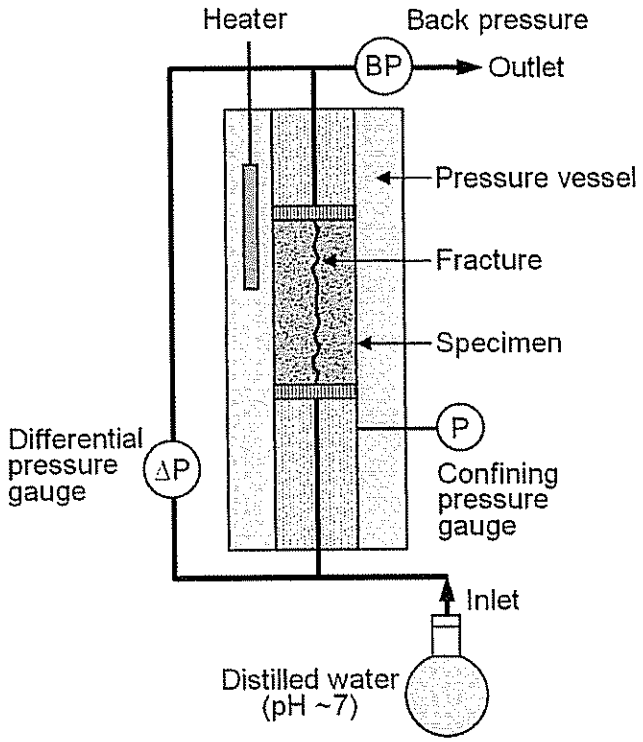

Figure 1. Schematic illustration of experimental setup for flow-through experiment.

× 89.5 mm length) containing a single diametral fracture along its cylindrical axis. Arkansas novaculite is > 99.5 % quartz [Lee *et al.*, 1991], and distilled water was used as a permeant. End-to-end pressure differential is continuously recorded along the sample with prescribed flow rates in the range 1.0 – 0.0625 mL/min applied at 1.38 MPa (200 psi) effective stress, that may be converted to hydraulic aperture [e.g., Gangi, *1978;* Tsang and Witherspoon, 1981]. The sample was held at uniform temperatures in the range 20 – 120 °C. Experimental conditions during the entire length of the experiment (3150 hrs) are given in Table 1. In addition, the fluid samples were taken from the flow outlet at regular intervals (one sample per day) to determine effluent Si concentrations. After the termination of the flow-through experiment the aperture distribution within a fracture was measured first by X-ray CT, and then by destructive casting with Wood's metal.

Table 1. Experimental conditions.

Time [hr]	Temperature [°C]	Flow rate [mL/min]	Flow Direction
0 – 121	20	1.0	Original
121 – 380	20	0.5	Original
380 – 858	20	0.25	Original
858 – 930	20	0.0	–
930 – 1266	20	0.25	Original
1266 – 1292	20	0.125	Original
1292 – 1494	20	0.125	Reversed
1494 – 1869	20	0.0625	Original
1869 – 2255	40	0.0625	Original
2255 – 2875	80	0.0625	Original
2875 – 3150	120	0.125	Original

Experimental Results and Analyses

The evolution of permeability within a fracture may be attributed to the redistribution of mineral mass from contacting asperities and/or fracture void surfaces. Dissolution at the contacting asperities may result in a net-decrease in fracture aperture, provided this effect outstrips gaping induced by dissolution from the fracture surface. These dynamic processes are constrained from concurrent measurements of evolving aperture, mineral efflux, and imaging by X-ray CT, anchored to final destructive casting of the fracture using Wood's metal.

Evolution of Fracture Aperture

Figure 2a shows the evolving change in normalized differential pressure with time. The hydraulic aperture decreased monotonically from 18.5 to 9.6 μm during the first 1292 hrs of the test, with a reduction in the flow rates from 1.0 to 0.25 mL/min. After the flow direction was reversed at 1292 hr, the aperture reduced to 7.5 μm during 1292 – 1494 hr. Abrupt

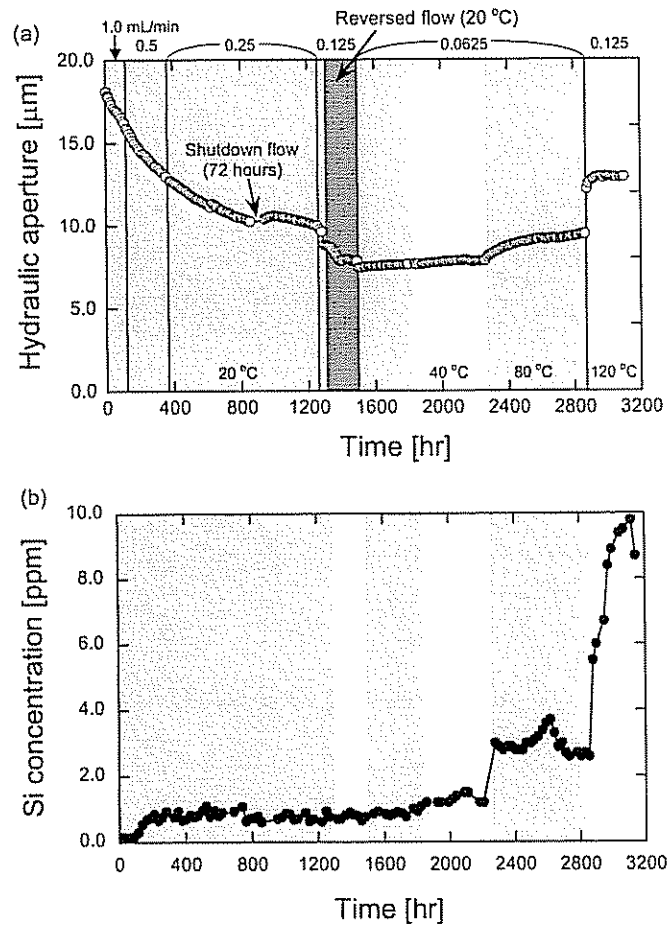

Figure 2. Experimental measurements; (a) Changes in hydraulic aperture with time and (b) Si concentration with time.

decreases in fracture aperture were apparent when the flow was reversed at both 1292 and 1494 hr. This instantaneous closure in aperture is interpreted as a switch of the stress distribution. Effective stress at the sample inlet is smaller than that at the outlet because of the higher pore pressure applied at the inlet; this may correspondingly accommodate a larger aperture at the inlet. Switching of flow directions is correlated with the switching of stress distributions, and accordingly this may reduce aperture around the previous inlet (i.e., outlet after reverse of the flow), resulting in net-closure within the fracture.

Subsequently, the hydraulic aperture switched to a monotonic increase as temperatures were elevated for the remainder of the experiment. The switch from aperture-reduction to -increase has been previously reported in carbonates [Polak *et al., 2004*]. The phenomenon of switching between permeability-reduction to permeability-increase is likely due to a switch in the dominant process of mineral redistribution – from beneath the bridging asperities to the faces of the fracture. Dissolution at contacting asperities is stress-dependent [e.g., Rutter, *1976;* Raj, *1982*]. The stress at the asperities decreases with an increase in contact area as the fracture closes, reducing the mass rate of removal from beneath the asperities relative to that etched by free-face dissolution. This correspondingly results in a change from net closure to net gaping, with a concomitant change in permeability.

Surface Dissolution

The change in measured effluent Si concentration is shown in Figure 2b. Concentrations measured at 20 °C were in the range 0.13 to 1.20 ppm with a mean of 0.76 ppm. The mean values at elevated temperatures increased with the increase of temperature; their values at 40, 80, and 120°C were 1.30, 2.96, 8.10 ppm, respectively. Measured Si concentrations are clearly temperature dependent, and show the Arrhenius-type dependence (Figure 3). The activation energy of Si solubility obtained in this study is 22.2 kJ mol^{-1}, which is congruent

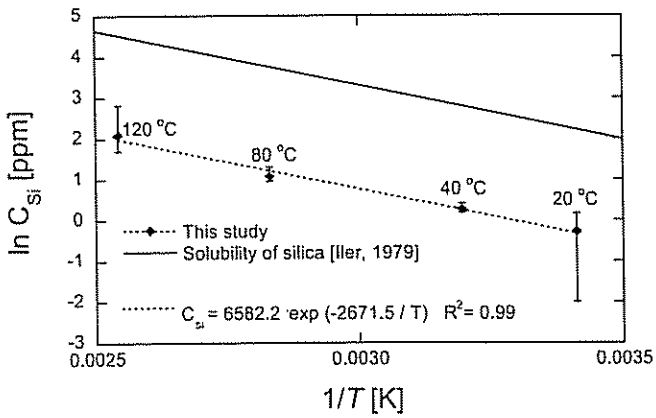

Figure 3. Relation between Si concentration and temperature. Solid dots represent mean measured concentrations and error bars show the maximum and minimum concentrations at the temperatures. Measured Si concentration is strongly correlated to temperature by an Arrhenius-type relation. Solid line represents the solubility curve by Iler [1979] with activation energy of 21.7 kJ mol^{-1}, and dotted line is the regression curve for the measured with apparent activation energy of 22.2 kJ mol^{-1}.

with Iler [1979] at 21.7 kJ mol^{-1}. In contrast, the measured concentrations are much lower than Si solubilities (~9, 17, 44, 94 ppm at 20, 40, 80, 120 °C, respectively [Iler, 1979]) due to the short residence time of the fluid within the fracture (ca. a few tens of seconds). This implies that precipitation remained inactive within the fracture throughout the 3150 hr duration of the experiment, and suggests that net dissolution prevailed throughout.

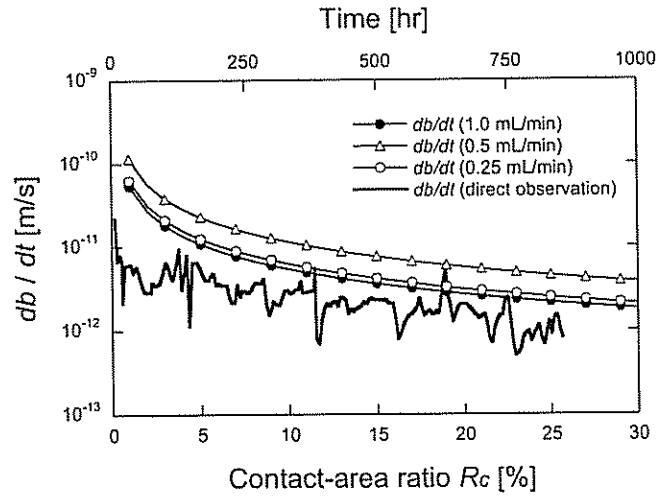

Figure 4. Comparison of change in rate of aperture reduction, *db/dt*. Solid line represents the change in direct observation of *db/dt* with time (0 – 858 hr). Slid circles, open triangles, and open circles represent predictions by Eq. (2) at different flow rates in the range 1.0 to 0.25 mL/min.

The dominant role of dissolution at contacting asperities has been examined in terms of the rate of aperture reduction, *db/dt*, [Polak *et al.*, 2003; Yasuhara *et al.*, 2004] recorded from flow-through tests where independent estimates of the hydraulic fracture aperture are derived from the effusing fluid and mineral flux. Hydraulically measured aperture reduction rates, *db/dt*, in the first 858-hr duration are in the range 2.0×10^{-11} to 5.0×10^{-13} m/s as shown in Figure 4. The hydraulically measured rates may be augmented by estimates from mineral mass efflux, where an assumption is made regarding the contact-area ratio, R_c, as,

$$\frac{db}{dt} = \frac{Q \cdot C_{SiO2}}{R_c \cdot A_f \rho_g} , \qquad (1)$$

where A_f is the total fracture area ($A_f = 8.95\times10^{-3}$ m^2) and ρ_g is grain density (2650 kg m^{-3} for quartz). Varying the unmeasured fractional contact area in the range 1 to 30 %, the rates of aperture reduction, *db/dt*, may be determined from the mean Si concentrations, C_{Si}, of 0.18, 0.77, and 0.87 ppm, equivalent to SiO_2 concentration, C_{SiO2}, of 0.39, 1.63, and 1.86 ppm, at prescribed flow rates, Q, of 1.0, 0.5, and 0.25 mL/min, respectively. These estimates, in the range 1.1×10^{-10} to 2.0×10^{-12} m/s, are close to, but slightly higher than those recovered from the hydraulic measurements. This mismatch may result either from an unaccounted contribution of dissolution at the fracture void walls, or from an underestimate of assumed fracture contact area.

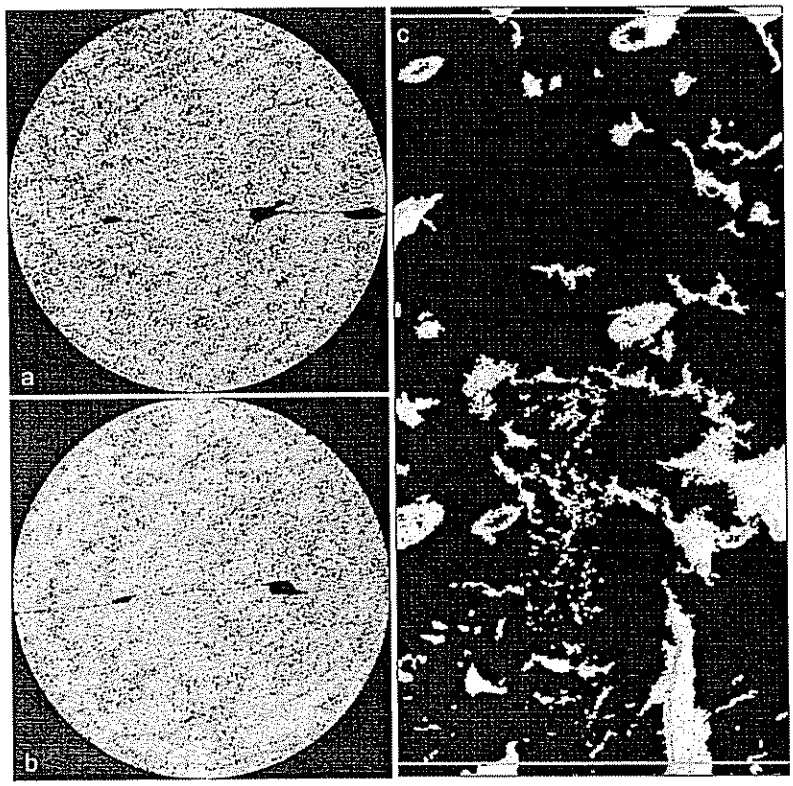

Figure 5. Images of the CT scan obtained at the end of the flow experiment. The left images show two CT images of the rock sample taken at the top (a) and bottom (b) parts of the sample. The fracture is clearly visible at the center of the image where the large black pores are areas where pieces of the fracture surface was missing. The right image (c) shows a 3D reconstruction of 1477 CT images representing a complete view of the fracture surface. The white areas are fracture voids demarked with a threshold CT number of 2650.

X-ray CT Analysis

The left side of Figure 5 shows two CT images taken at the termination of the flow experiment from the upper (a) and lower (b) parts of the rock sample. The fracture is clearly visible in the center of the image (marked in black). The black spots in the rocks matrix are areas where the density of the rock is lower relative to the rest of the matrix. These regions are not interconnected and exert no influence on the in-fracture flow. The right side of Figure 5 shows a 3D reconstruction of 1477 images representing a complete view of the rock fracture. The two lines demark the scans where two images shown on the left were captured. The white regions in the 3D reconstruction are fracture voids demarked with a threshold CT number of 2650. The 3D reconstruction suggests that there are no continuous paths within the fracture, however this aberration results from the finite resolution of the imaging (50×50×60.6 μm). We may calculate the total volume of the fracture (white area) and estimate the average fracture aperture of the whole rock sample. The total fracture volume was calculated to be 390 mm^3, which for the scanned area of 4200 mm^2 gives an average fracture aperture of 95 μm. The average fracture aperture estimated from the CT images is larger than the hydraulic aperture at the end of experiment (i.e., 13 μm), which may be attributed to the chosen threshold CT number. However, the estimated aperture hereinabove is still plausible and indexes to the actual value evaluated from the flow-through experiment although the CT resolution is insufficiently high.

Wood's Metal Fracture

Following the injection of Wood's metal into the fracture, the Wood's metal cast was removed from the novaculite by immersing the cast-ingot inside a bath filled with hydrofluoric acid (~25 wt.%). Immersion for 166 hrs removed the surrounding rock matrix, although a small portion of the fracture top was bowed (Figure 6a). It is apparent that Wood's metal propagated throughout the fracture except not into the regions in contact. No preferential flow paths are apparent within the cast, which is congruent with the CT observations. Importantly, the alloy fracture cast enables the contact area to be quantitatively evaluated from the digitized black-and-white image (~65 % of the whole fracture) as shown in Figure 6b. The calculated contact-area ratio is 14.5 % and may be consistent with the plausible amount in rock fractures [e.g., Tang and Witherspoon, 1981; Pyrak-Nolte *et al.*, 1987].

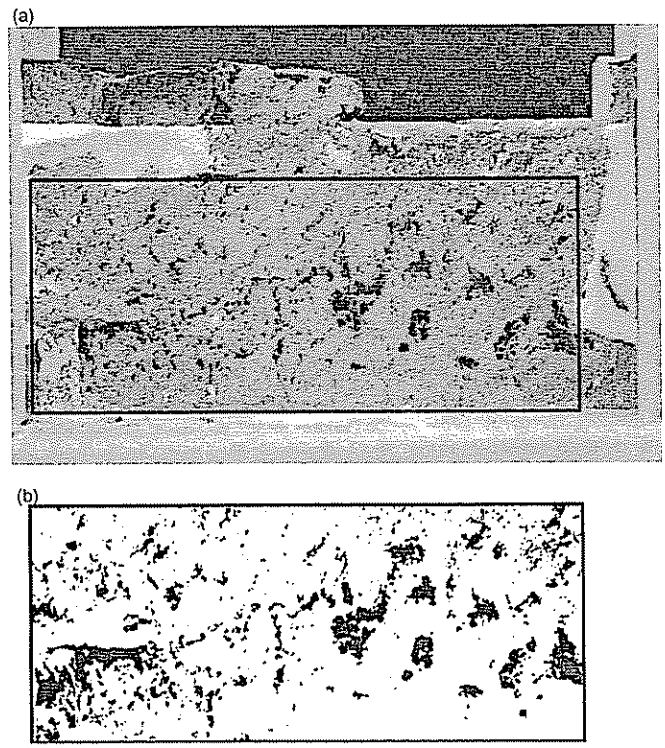

Figure 6. Wood's metal fracture extracted through chemical dissolution using hydrofluoric acid; (a) whole fracture – white region is residual rock sample, and (b) black-and-white representation of the boxed area in (a). Black area represents regions in contact and calculated contact area is 14.5 %.

Conclusions

Experimental measurements of fluid and mineral mass effluxes, constrained by non-destructive imaging by X-ray CT, and by destructive imaging of a fracture cast, allow the evolution of fracture aperture to be followed. For isothermal flow at low temperature (20°C), the fracture closed monotonically as the bridging asperities are progressively removed. This amounts to a 60 % reduction in fracture aperture over the initial 1500 hr duration of the experiment. Subsequently, free-face dissolution dominates over the effects of dissolution at contacting asperities, and results in an augmentation in fracture aperture. The rate of gaping increases with an increase in temperature, corresponding to the exponential (or Arrhenius-type) dependence on the mineral effluxes measured. The activation energy constrained in this work is 22.2 kJ mol^{-1}, congruent with that obtained from Iler [1979] (i.e., 21.7 kJ mol^{-1}).

The post-experiment observations by the X-ray CT and Wood's metal cast revealed the detailed distribution of local apertures and regions in contact within the fracture. These independent measurements imply no presence of a preferential flow path generated during the experiments – despite the hydraulic signal that suggests the contrary. The average aperture evaluated from the CT images is sevenfold larger than the hydraulic aperture at the end of the experiment. This mismatch is likely due to limitations in the resolution of the CT imaging, and in the choice of threshold CT number.

The measured Si concentrations are significantly below equilibrium solubilities at all temperatures, due to the high prescribed flow rates, and the resulting short residence time in the fracture. Examining this far-from-equilibrium behavior is important in considering the rates and magnitudes of permeability-enhancement within rock fractures stimulated by chemical permeants in geothermal and petroleum reservoirs. The current experimental measurements showed permeability degradation first and then accelerating enhancement with an increase in temperature, but the important factors (i.e., temperature, stress, and chemistry in the pore fluid) triggering this switching remain insufficiently constrained. Thus, further detailed investigations are required to achieve more realistic understanding on the evolution in fracture permeability mediated by coupled thermal, hydraulic, mechanical, and chemical processes.

Acknowledgements

This work has been supported by grants DOE-BES-DE-FG02-00ER15111, DOE-DE-FG36-04GO14289, and ARC DP0209425. This support is gratefully acknowledged.

References

Dobson, P. F., T. J. Kneafsey, E. L. Sonnenthal, N. Spycher, and J. A. Apps (2004), Experimental and numerical simulation of dissolution and precipitation: implications for fracture sealing at Yucca Mountain, Nevada, *J. Contam. Hydrol., 62-63*, 459-476.

Durham, W. B., W. L. Bourcier (2001), and E. A. Burton, Direct observation of reactive flow in a single fracture. *Water Resour. Res., 37*, 1-12.

Gangi, A. F. (1978), Variation of whole and fractured porous rock permeability with confining pressure, *Int. J. Rock Mech. Min. Sci. Geomech. Abstr., 15*, 249-257.

Higlers, C. and E. Tenthorey (2004), Fracture sealing of quartzite under a temperature gradient: experimental results, *Terra Nova, 16(4), 173-178.*

Iler, R. K. (1979), *The Chemistry of Silica*, John Wiley, New York.

Kanagawa, K., S. F. Cox, and S. Zhang (2000), Effects of dissolution-precipitation processes on the strength and mechanical behavior of quartz gouge at high-temperature hydrothermal conditions, *J. Geophys. Res.*, 105(B5), 11,115-11,126.

Lee, V.W., S.J. Mackwell, and S.L. Brantley (1991), The effect of fluid chemistry on wetting textures in novaculite. *J. Geophys. Res.* 96(B6):10023-10037.

Lin, W., J. Roberts, W. Glassley, and D. Ruddle (1997), Fracture and matrix permeability at elevated temperatures, Workshop on significant issues and available data, Near-field/Altered-zone coupled effects expert elicitation project, San Francisco, November.

Liu, X., A. Ormond, K. Bartko, Y. Li, and P. Ortoleva (1997), A geochemical reaction-transport simulator for matrix acidizing analysis and design, *J. Pet. Sci. and Eng., 17*, 181-196.

Moore, D. E., D. A. Lockner, J. D. Byerlee (1994), Reduction of permeability in granite at elevated temperatures, *Science, 265*, 1558-1561.

Morrow, C. E., D. E. Moore, and D. A. Lockner (2001), Permeability reduction in granite under hydrothermal conditions, *J. Geophys. Res., 106*, 30,551-30,560.

Palmer, A. N., Origin and morphology of limestone caves, *Geol. Soc. Am. Bull., 103*, 1-21, 1991.

Polak, A., D. Elsworth, H. Yasuhara, A. Grader, and P. Halleck (2003), Permeability reduction of a natural fracture under net dissolution by hydrothermal fluids, *Geophys. Res. Lett., 30(20), 2020, doi:10.1029/2003GL017575.*

Polak A., D. Elsworth, J. Liu, and A. S. Grader (2004), Spontaneous switching of permeability changes in a limestone fracture with net dissolution, *Water Resour. Res., 40*, W03502, doi:10.1029/2003WR002717.

Pyrak-Nolte, L. J., L. Myer, N. G. W. Cook, and P. A. Witherspoon (1987), Hydraulic and mechanical properties of natural fractures in low permeability rock, *Proc. Int. Cong. Int. Soc. Rock Mech.*, Montreal, 225– 231.

Raj, R. (1982), Creep in polycrystalline aggregates by matter transport though a liquid phase, *J. Geophys. Res., 87*(B6), 4731-4739.

Rutter, E.H. (1976), The kinetics of rock deformation by pressure solution, *Philos. Trans., R. Soc. London, Ser. A, 283*, 203-219.

Tenthorey, E., S. F. Cox, and H. F. Todd (2003), Evolution of strength recovery and permeability during fluid-rock reaction in experimental fault zones, *Earth. Planet. Sci. Lett., 206, 161-172.*

Tsang, Y. W. and P. A. Witherspoon (1981), Hydromechanical behavior of a deformable rock fracture subject to normal stress, *J. Geophys. Res.*, 86, 9287-9298.

Yasuhara, H., D. Elsworth, and A. Polak, A (2003), A mechanistic model for compaction of granular aggregates moderated by pressure solution, *J. Geophys. Res., 108*, B11, 2530, doi:10.1029/2003JB002536.

Yasuhara, H., D. Elsworth, and A. Polak, A (2004), Evolution of permeability in a natural fracture: Significant role of pressure solution, *J. Geophys. Res., 109*, B03204, doi:10.1029/2003JB002663.